Generalized Discrete-Time Equivalent Model for the Dynamic Simulation of Regional Power Grids

Fu Shen, *Student Member*, *IEEE*, Ping Ju, *Senior Member*, *IEEE*, Mohammad Shahidehpour, *Fellow*, *IEEE*, Zhiyi Li, *Member*, *IEEE* and Xueping Pan

Abstract— **The introduction of an equivalent model for regional power grids in a large-scale power system with complex loads is essential for reducing the computation burden in real-time dynamic analyses. In this paper, we propose a generalized discrete-time equivalent model (GDEM) for simulating the physical characteristics of a regional power grid. GDEM facilitates the interconnection of equivalent models for representing regional power grids and improving the accuracy and speed in dynamic simulations of large-scale power systems. The paper first investigates the inherent relationships among coefficients in the discrete-time models of synchronous generators and composite loads so as to guide the estimation of coefficients of the GDEM for regional power grids. The paper then develops relationships among coefficients associated with GDEM for a regional power grid. The GDEM that is formed by combining discrete-time models of synchronous generators and composite loads represents specific dynamic characteristics of regional power grids. Numerical experiments are conducted by simulating ground faults in the China Electric Power Research Institute system, and the accuracy of the proposed GDEM is verified by analyzing the simulation results. In addition, the paper has applied GDEM to study the regional power grid of central China, which validates the use of GDEM in practical power system analyses.**

Index Terms—**Large-scale power system operation, discrete-time equivalent model for regional power grids, regional model.**

NOMENCLATURE

Indices	
i	Index for coefficients
K	Index for discrete time steps
Symbols	
Δ	Incremental value
$_0$	Subscript for steady state
Parameters	
$\dot{E}'$	Transient voltage
$\dot{U}$	Terminal voltage
$\dot{I}$	Terminal current
U	Amplitude of the bus voltage
I_d, I_q	Currents of *d*-axis and *q*-axis
U_d, U_q	Voltage of *d*-axis and *q*-axis
E_{fd}	The terminal voltage of excitation
I_{gr}, I_{gj} I_{gr}', I_{gj}'	Real and imaginary currents of generator
U_{gr}, U_{gj}	Real and imaginary voltages of generator
I_{cr}, I_{cj}	Real and imaginary currents of composite load
I_r, I_j	Real and imaginary currents flowing into the regional power grid
φ	Bus voltage phase angle
T_d', T_d''	Short-circuit transient and sub-transient time constants of *d*-axis
f_x, f_y	Variables in *x*-*y* coordinates
f_d, f_q	Variables in *d*-*q* coordinates
T_{d0}', T_{d0}''	Open-circuit transient and sub-transient time constants of *d*-axis
T_D'	Short-circuit transient time constant of D-branch
T_{D0}''	Open-circuit transient time constant of D-branch
T_q''	Short-circuit sub-transient time constant of *q*-axis
T_{q0}''	Open-circuit sub-transient time constant of *q*-axis
D	Damping coefficient
δ	Angle of the generator
ω	Angular velocity of rotor
R_s, R_r	Resistance of stator and rotor
X_s, X_r	Reactance of the stator and rotor
X	Steady state reactance
X'	Transient reactance
X_m	Exciting reactance
x_{ffd}, x_{ffq}	Equivalent excitation reactance of *d*-axis and *q*-axis
x_{11d}, x_{11q}	Positive sequence equivalent reactance of *d*-axis
x_{ad}	Reactance of armature reaction of *d*-axis
x_d	Reactance of *d*-axis
x_d', x_d''	Transient and sub-transient reactance of *d*-axis
R_{fd}, R_{fq}	Equivalent excitation resistance of *d*-axis and *q*-axis
R_{1d}, R_{1q}	Positive sequence equivalent resistance of *d*-axis and *q*-axis
Ψ_d, Ψ_q	Flux linkages of *d*-axis and *q*-axis
u_f	Excitation winding voltage
h	Sampling time step
Variables	
$X_d(s)$, $X_q(s)$	Inductances of *d*-axis and *q*-axis
θ_{gi} and $\theta_{g\varphi i}$	Both are the discrete-time model coefficient of the synchronous generator
θ_{ci}	Discrete-time model coefficient of composite load
θ_i	Discrete-time model coefficient of regional power grid
s	Laplace transformation
z	Z transformation

Other notations are defined in the text.

This work was supported in part by the "111" project of "Renewable Energy and Smart Grid" (B14022), the National Key Basic Research Program of China (973 Program) (2013CB228204), and the 2016 Ordinary University Graduate Student Scientific Research Innovation Project of Jiangsu Province (2016B44314). F. Shen, P. Ju and X. Pan are with the School of Energy and Electrical Engineering, Hohai University, Nanjing, China (shenfu@hhu.edu.cn; pju@hhu.edu.cn; xueping_pan@163.com). Z. Li and M. Shahidehpour are with the Electrical and Computer Engineering Department, Illinois Institute of Technology, Chicago, USA (zhiyi.li@hawk.iit.edu; ms@iit.edu).

I. INTRODUCTION

LARGE power grids are often operated through coordinated controls of a hierarchy of regional power grids. Individual regional power grids equipped with energy management systems (EMSs) establish equivalent models for their external regional systems with numerous challenging tasks for data exchanges among regional power system models [1]–[3], which has consistently threatened the stability of power systems [4],[5].

Recently, several studies have proposed equivalent models for regional power systems [6]-[7]. The equivalent models that were widely adopted for maintaining the dynamic characteristics of regional power grids represented three categories of coherent-based models [8],[9], analytical models [10],[11], and estimated equivalent models [12],[13]. In most cases, an aggregated generator was used to represent multiple generators in the equivalent model of a regional power grid and an equivalent load was adopted to represent a multitude of loads [14]–[16].

With the additional uncertainty introduced in power system operations and the increasing penetration of renewable energy resources into regional power grids, the attainment of an equivalent model for a regional power grid has become more cumbersome [17],[18], leading to strong nonlinearities in regional power grids [19]. In [20], a seventh-order nonlinear quasi-state space model was derived for an active distribution network. In [21], a second-order transfer function was used as a dynamic equivalent model for a distribution network. In [22], the artificial neural network (ANN) method was introduced to represent a model for a regional power grid. However, the equivalent model depended on the operating state of the regional power grid for estimating ANN weights.

It is difficult to obtain an equivalent representation of regional power grids for dynamic stability analyses as power systems are inherently nonlinear and analytical models are generally lacking for equivalent representations of such nonlinear equations [23]. Ref. [24] proposed a semi-implicit formulation of differential-algebraic equations (DAEs) describing power system models for transient stability analyses, which reduce computation burdens and increase the sparsity of the Jacobian matrix of the power system. Ref. [25] described the Power System Analysis Toolbox (PSAT), an open software package for analysis and design of small to medium size electric power systems. A regional power grid equivalent was often represented by a static load, which was a conservative model for embodying the power system operation in critical conditions such as the northeast blackout of 2003 in the United States. Therefore [26] proposed a large power systems equivalent represented by an aggregated generator, which characterizes coherent combinations of strongly connected machines in an area after the northeast blackout; however, the aggregated generator did not embody all typical types of loads.

The power system model represents the integration of smaller models for regional power grids to address the operation of the integrated power system that cannot be represented by individual smaller models. The power system model integration including a hierarchy of regional power grids are interconnected with external regional models for dynamic simulations. Ref. [27] presented the characteristic of a complex high-order continuous system based on an all-coefficient adaptive control method applied to the integrated power system model. Yet regional power grids cannot strictly satisfy the required condition that the external equivalent model parameters be time-independent.

An equivalent model that is universally applicable to regional power grids with diverse compositions is conducive to the assembly of the models of power system regions for real-time analyses that guide the secure operation of the whole power system. Dynamic components in a regional power grid usually include generators and induction motors. Accordingly, the generalized discrete-time model of a regional power grid can be derived based on discrete-time models of synchronous generators and composite loads, including various types of loads.

This paper proposed GDEM for a regional power grid based on discrete-time models of synchronous generators and composite loads consisted by induction motor load and static load as shown in Fig. 1, which is regional power grid. Fig. 1 (a) is original regional power grid and Fig. 1(b) is regional power grid representation, where *G* is a generator, *M* is induction motor load, including the typical type of load. GDEM considers the terminal voltage of the boundary bus and the injected current by the external grid as input and output state variables in each regional power system, respectively, which is different from the previous methods for developing the power system dynamic equivalence (e.g., [8]–[13]). Therefore, the practicability of GDEM is on representing regional power grids which consist of dynamic components (e.g., synchronous generators, induction motors) or static components (e.g., lights).

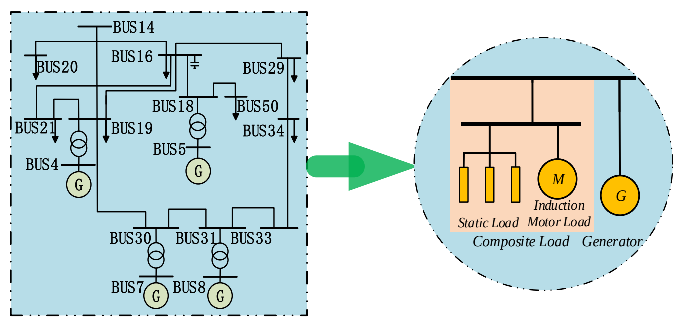

(a) (b)

Fig. 1. Regional power grid (a) Original regional power grid (b) Regional power grid representation

The contributions of this paper are listed as follows:

1) The paper has proposed GDEM for a regional power grid, which can be derived based on discrete-time models of individual synchronous generators (or an equivalent aggregated generator) and individual composite loads (or an equivalent aggregated composite loads).

2) GDEM investigates the inherent relationship among coefficients of the discrete-time models of synchronous generators and composite loads so as to guide the estimation of coefficients for representing those components in regional power grids.

3) The paper demonstrates analytically as well as via simulations that the sum of output state coefficients in the regional power grid model is approximately equal to 1, and the sum of input state coefficients is approximately equal to 0 in GDEM. On the one hand the relationship among coefficients could provide a theoretical basis for validating GDEM

parameters; on the other hand, the relationship among coefficients reduces the number parameters to be identified.

4）The paper studies the regional power grid of central China, using GDEM, which validates the use of GDEM in practical applications. The broader applications of GDEM are also discussed in the paper.

The remainder of this paper is organized as follows. First, discrete-time models are derived for a synchronous generator and a composite load in Sections II and III, respectively. Then Section IV presents a GDEM of a regional power grid based on the discrete-time models of generators and composite loads through the weighted sum method. The modeling steps for GDEM and case studies are considered in Section V to verify the accuracy of the proposed model. Finally, Section VI concludes this paper.

II. Discrete-time Model of a Synchronous Generator

Assume that there exists an equivalent winding in both *d*-axis and *q*-axis of a synchronous generator, where flux linkages of *d*-axis and *q*-axis are expressed as [28],[29],

$$\begin{cases} \psi_d = G(s)u_f - X_d(s)i_d \\ \psi_q = -X_q(s)i_q \end{cases} \tag{1}$$

Here, *G(s)* is the stator to field voltage transfer function [29]. $X_d(s)$ and $X_q(s)$ are expressed by,

$$\begin{cases} X_d(s) = X_d \dfrac{T_d''T_d's^2 + (T_D' + T_d')s + 1}{T_{d0}''T_{d0}'s^2 + (T_{D0}' + T_{d0}')s + 1} \\ X_q(s) = X_q \dfrac{T_q''s + 1}{T_{q0}''s + 1} \end{cases} \tag{2}$$

The armature resistance *R* is generally small enough to be ignored. The impedances are stated in (3) when the automatic voltage regulator (AVR) is applied,

$$\begin{cases} X_d(s) = -\dfrac{1}{\Delta I_d(s)}\Delta U_q(s) + \dfrac{1}{\Delta I_d(s)}\Delta G(s)\Delta E_{fd}(s) \\ X_q(s) = \dfrac{1}{\Delta I_q(s)}\Delta U_d(s) \end{cases} \tag{3}$$

Accordingly, (3) is rewritten as,

$$\begin{bmatrix} \Delta I_d(s) \\ \Delta I_q(s) \end{bmatrix} = \begin{bmatrix} \dfrac{-1}{X_d(s)} & 0 \\ 0 & \dfrac{1}{X_q(s)} \end{bmatrix} \begin{bmatrix} \Delta U_q(s) \\ \Delta U_d(s) \end{bmatrix} + \begin{bmatrix} \dfrac{\Delta G(s)\Delta E_{fd}(s)}{X_d(s)} \\ 0 \end{bmatrix} \tag{4}$$

Quantities in *dq* coordinates are transformed to those in *xy* coordinates given in the Fig. 2. Using *dq-xy* coordinates in Fig. 2, we can get

$$f_d + jf_q = (f_x + jf_y)e^{j(\frac{\pi}{2}-\delta)} \tag{5}$$

Through the transformation, we rewrite the (5) as,

$$\begin{bmatrix} f_x \\ f_y \end{bmatrix} = \begin{bmatrix} \sin\delta & \cos\delta \\ -\cos\delta & \sin\delta \end{bmatrix} \begin{bmatrix} f_d \\ f_q \end{bmatrix} \tag{6}$$

When the transformation matrix $\begin{bmatrix} \sin\delta & \cos\delta \\ -\cos\delta & \sin\delta \end{bmatrix}$ in (6) is applied to (4), we have

$$\begin{bmatrix} \Delta I_{gr}(s) \\ \Delta I_{gj}(s) \end{bmatrix} = \begin{bmatrix} a_{11} & a_{12} \\ a_{21} & a_{22} \end{bmatrix} \begin{bmatrix} \Delta U_{gr}(s) \\ \Delta U_{gj}(s) \end{bmatrix} \tag{7}$$

where

$$a_{11} = \frac{1}{2}\sin 2\delta_0 \left[\frac{1}{X_d(s)} - \frac{1}{X_q(s)} \right],$$

$$a_{12} = \frac{1}{X_d(s)} + \left[\frac{1}{X_q(s)} - \frac{1}{X_d(s)} \right] \frac{\cos 2\delta_0 - 1}{2},$$

$$a_{21} = \left[\frac{1}{X_q(s)} - \frac{1}{X_d(s)} \right] \frac{\cos 2\delta_0 - 1}{2} - \frac{1}{X_q(s)},$$

$$a_{22} = \frac{1}{2}\sin 2\delta_0 \left[\frac{1}{X_q(s)} - \frac{1}{X_d(s)} \right].$$

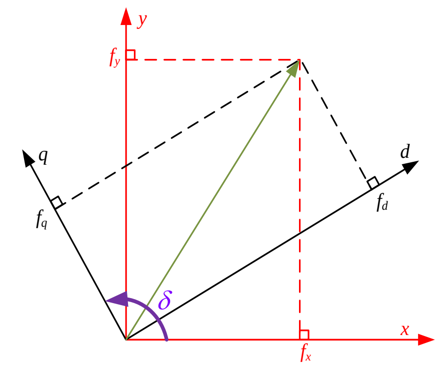

Fig. 2. *dq-xy* coordinates

As the model accuracy suffers and the number of parameters is increased when bus voltage phase angles are explicitly expressed in (7). Accordingly, the bus voltage phase angle is ignored for facilitating the model derivation, and (7) is simplified as

$$\begin{cases} \Delta I_{gr}(s) = \dfrac{1}{2}\sin 2\delta_0 \left[\dfrac{1}{X_d(s)} - \dfrac{1}{X_q(s)} \right] \Delta U(s) \\ \Delta I_{gj}(s) = \left\{ \begin{array}{l} \dfrac{1}{2}\cos 2\delta_0 \left[\dfrac{1}{X_q(s)} - \dfrac{1}{X_d(s)} \right] - \\ \dfrac{1}{2}\left[\dfrac{1}{X_q(s)} - \dfrac{1}{X_d(s)} \right] - \dfrac{1}{X_q(s)} \end{array} \right\} \Delta U(s) \end{cases} \tag{8}$$

The transfer functions relating the generator's current to its voltage are derived as,

$$\frac{\Delta I_{gr}(s)}{\Delta U(s)} = \frac{a_{gr}s^3 + b_{gr}s^2 + c_{gr}s + d_{gr}}{e_{gr}s^3 + f_{gr}s^2 + g_{gr}s + h_{gr}} \tag{9}$$

$$\frac{\Delta I_{gj}(s)}{\Delta U(s)} = \frac{a_{gj}s^3 + b_{gj}s^2 + c_{gj}s + d_{gj}}{e_{gj}s^3 + f_{gj}s^2 + g_{gj}s + h_{gj}} \tag{10}$$

where detailed expressions of parameters are presented in Appendix A.

The bilinear transformation is a nonlinear mapping method that compresses the infinite frequency range to a finite one to avoid the spectrum aliasing caused by the continuous-discrete transformation [25]. According to the bilinear transformation applied to (9) and (10), we have

$$\begin{aligned} &\Delta I_{gr}(k+3) = \theta_{g1}\Delta I_{gr}(k+2) + \theta_{g2}\Delta I_{gr}(k+1) + \theta_{g3}\Delta I_{gr}(k) + \\ &\theta_{g4}\Delta U(k+3) + \theta_{g5}\Delta U(k+2) + \theta_{g6}\Delta U(k+1) + \theta_{g7}\Delta U(k) \end{aligned} \tag{11}$$

$$\begin{aligned} &\Delta I_{gj}(k+3) = \theta_{g8}\Delta I_{gj}(k+2) + \theta_{g9}\Delta I_{gj}(k+1) + \theta_{g10}\Delta I_{gj}(k) + \\ &\theta_{g11}\Delta U(k+3) + \theta_{g12}\Delta U(k+2) + \theta_{g13}\Delta U(k+1) + \theta_{g14}\Delta U(k) \end{aligned} \tag{12}$$

where detailed expressions of all parameters are presented in Appendix B. The real-part coefficients θ_{g1}, θ_{g2}, θ_{g3}, θ_{g4}, θ_{g5}, θ_{g6}, θ_{g7} and the imaginary-part coefficients θ_{g8}, θ_{g9}, θ_{g10}, θ_{g11}, θ_{g12}, θ_{g13}, θ_{g14} in (11) and (12), respectively, are related to time constants T_d', T_{d0}', T_d'', T_{d0}'', T_D', T_{D0}', T_q'', T_{q0}'' and the sampling time h (where $s = \frac{2}{h}\frac{1-z^{-1}}{1+z^{-1}}$) in the bilinear transformation. In turn, the time constants are dependent on reactance x_{ffd}, x_{ffq}, x_{11d}, x_{11q}, x_{ad}, x_d, x_d', x_d'' and resistances R_{fd}, R_{fq}, R_{1d}, R_{1q}. Hence, the discrete-time model of a synchronous generator is dependent on its physical characteristics.

The following relationships are observed in (11) and (12) when sampling time h is small,

$$\theta_{g1}+\theta_{g2}+\theta_{g3} = \frac{-7h_{gr}h^3+2g_{gr}h^2+4f_{gr}h+8e_{gr}}{h_{gr}h^3+2g_{gr}h^2+4f_{gr}h+8e_{gr}} \approx 1 \tag{13}$$

$$\theta_{g4}+\theta_{g5}+\theta_{g6}+\theta_{g7} = \frac{8d_{gr}h^3}{h_{gr}h^3+2g_{gr}h^2+4f_{gr}h+8e_{gr}} \approx 0 \tag{14}$$

$$\theta_{g8}+\theta_{g9}+\theta_{g10} = \frac{-7h_{gj}h^3+2g_{gj}h^2+4f_{gj}h+8e_{gj}}{h_{gj}h^3+2g_{gj}h^2+4f_{gj}h+8e_{gj}} \approx 1 \tag{15}$$

$$\theta_{g11}+\theta_{g12}+\theta_{g13}+\theta_{g14} = \frac{8d_{gj}h^3}{h_{gj}h^3+2g_{gj}h^2+4f_{gj}h+8e_{gj}} \approx 0 \tag{16}$$

It is shown here that the sum of output state coefficients of a synchronous generator is approximately equal to 1, and the sum of input state coefficients is approximately equal to 0.

When the variation of bus voltage phase angle is considered, the transfer functions relating the generator current to its voltage magnitude and phase angle are derived as,

$$\Delta I_{gr}'(s) = G_{1gr}(s)\Delta U(s) + G_{2gr}(s)\Delta\varphi(s) \tag{17}$$

$$\Delta I_{gj}'(s) = G_{1gj}(s)\Delta U(s) + G_{2gj}(s)\Delta\varphi(s) \tag{18}$$

where $G_{1gr}(s)$ and $G_{2gr}(s)$ are the transfer functions of I_{gr}' with respect to U and φ. $G_{1gj}(s)$ and $G_{2gj}(s)$ are transfer functions of I_{gj}' with respect to U and φ.

According to the bilinear transformation applied to (17) and (18), we have

$$\begin{aligned}&\Delta I_{gr}'(k+3) = \theta_{g1}\Delta I_{gr}'(k+2) + \theta_{g2}\Delta I_{gr}'(k+1) + \theta_{g3}\Delta I_{gr}'(k) + \\ &\theta_{g4}\Delta U(k+3) + \theta_{g5}\Delta U(k+2) + \theta_{g6}\Delta U(k+1) + \theta_{g7}\Delta U(k) + \\ &\theta_{g\varphi1}\Delta\varphi(k+3) + \theta_{g\varphi2}\Delta\varphi(k+2) + \theta_{g\varphi3}\Delta\varphi(k+1) + \theta_{g\varphi4}\Delta\varphi(k)\end{aligned} \tag{19}$$

$$\begin{aligned}&\Delta I_{gj}'(k+3) = \theta_{g8}\Delta I_{gj}'(k+2) + \theta_{g9}\Delta I_{gj}'(k+1) + \theta_{g10}\Delta I_{gj}'(k) + \\ &\theta_{g11}\Delta U(k+3) + \theta_{g12}\Delta U(k+2) + \theta_{g13}\Delta U(k+1) + \theta_{g14}\Delta U(k) + \\ &\theta_{g\varphi5}\Delta\varphi(k+3) + \theta_{g\varphi6}\Delta\varphi(k+2) + \theta_{g\varphi7}\Delta\varphi(k+1) + \theta_{g\varphi8}\Delta\varphi(k)\end{aligned} \tag{20}$$

The detailed expressions are not stated here. However when the bus voltage phase angle is ignored in (11) and (12), we find that the number of model parameters is 14. When the bus voltage phase angle is considered in (19) and (20), we find that the number of model parameters increases to 22, which can be a computation burden. Correspondingly, the voltage phase angle variations are ignored in our study in order to facilitate the derivation and the simulation of the proposed model. The detailed analyses are provided in Section V.

III. Discrete-time Model of a Composite Load

A composite load consists of a static load and an induction motor connected in parallel [29]–[32], which is expressed as,

$$T_{d0}'\frac{d\dot{E}'}{dt} = -\dot{E}' + j(X-X')\dot{I} + j(\omega-1)\dot{E}'T_{d0}' \tag{21}$$

where $\dot{E}' = \dot{U} - (R_s + jX')$, $\dot{I} = (\dot{U}-\dot{E}')/(R_s+jX')$, $X = X_s + X_m$, $X' = X_s X_m/(X_s+X_m)$, $T_{d0}' = (X_r+X_m)/R_r$.

When the terminal voltage and the injected current of the composite load are considered as input and output variables, respectively, (21) is transformed as [33],

$$\begin{cases}\dfrac{dI_{cr}}{dt} = A_r I_{cr} + B_r I_{cj} + C_r U + G\dfrac{dU}{dt} \\ \dfrac{dI_{cj}}{dt} = A_j I_{cr} + B_j I_{cj} + C_j U - B\dfrac{dU}{dt}\end{cases} \tag{22}$$

where $A_r = -(1+B\Delta X)/T_{d0}'$, $B_r = \omega - 1 - G\Delta X/T_{d0}'$, $C_r = G/T_{d0}' - B(\omega-1)$, $A_j = -\omega+1+G\Delta X/T_{d0}'$, $B_j = -(1+B\Delta X)/T_{d0}'$, $C_j = B/T_{d0}' + G(\omega-1)$, $\Delta X = X - X'$, $G = R_s/(R_s^2+X'^2)$, $B = X'/(R_s^2+X'^2)$.

The frequency domain representation of (22) is obtained by applying the Laplace transformation to (22),

$$\begin{cases}s\Delta I_{cr}(s) = A_r\Delta I_{cr}(s) + B_r\Delta I_{cj}(s) + C_r\Delta U(s) + sG\Delta U(s) \\ s\Delta I_{cj}(s) = A_j\Delta I_{cr}(s) + B_j\Delta I_{cj}(s) + C_j\Delta U(s) - sB\Delta U(s)\end{cases} \tag{23}$$

Accordingly, transfer functions relating real and imaginary parts of injected current to terminal voltage is obtained as,

$$\frac{\Delta I_{cr}(s)}{\Delta U(s)} = \frac{B_rC_j - sB_rB + sC_r + s^2G - B_jC_r - sGB_j}{s^2 - sB_j - sA_r + A_rB_j - B_rA_j} \tag{24}$$

$$\frac{\Delta I_{cj}(s)}{\Delta U(s)} = \frac{A_jC_r + sA_jG + sC_j - s^2B - A_rC_j + sBA_r}{s^2 - sA_r - sB_j + A_rB_j - A_jB_r} \tag{25}$$

The following difference equations are obtained by applying the bilinear transformation to (18) and (19),

$$\begin{aligned}&\Delta I_{cr}(k+2) = \theta_{c1}\Delta I_{cr}(k+1) + \theta_{c2}\Delta I_{cr}(k) + \\ &\theta_{c3}\Delta U(k+2) + \theta_{c4}\Delta U(k+1) + \theta_{c5}\Delta U(k)\end{aligned} \tag{26}$$

$$\begin{aligned}&\Delta I_{cj}(k+2) = \theta_{c6}\Delta I_{cj}(k+1) + \theta_{c7}\Delta I_{cj}(k) + \\ &\theta_{c8}\Delta U(k+2) + \theta_{c9}\Delta U(k+1) + \theta_{c10}\Delta U(k)\end{aligned} \tag{27}$$

where detailed expressions of all parameters are presented in Appendix C.

The real-part coefficients θ_{c1}, θ_{c2}, θ_{c3}, θ_{c4}, θ_{c5} and the imaginary-part coefficients θ_{c6}, θ_{c7}, θ_{c8}, θ_{c9}, θ_{c10} in (26) and (27) are related to the composition of the composite load as well as the sampling time h. Hence, the discrete-time model of a composite load is dependent on its physical characteristics.

The following relationships among the coefficients in (26) and (27) are derived when h is small enough,

$$\theta_{c1}+\theta_{c2} = \frac{3h^2(B_rA_j - A_rB_j) - 2h(A_r+B_j) + 4}{h^2(A_rB_j - B_rA_j) - 2h(A_r+B_j) + 4} \approx 1 \tag{28}$$

$$\theta_{c3}+\theta_{c4}+\theta_{c5} = \frac{4h^2(B_rC_j - B_jC_r)}{h^2(A_rB_j - B_rA_j) - 2h(A_r+B_j) + 4} \approx 0 \tag{29}$$

$$\theta_{c6}+\theta_{c7} = \frac{3h^2(B_rA_j - A_rB_j) - 2h(A_r+B_j) + 4}{h^2(A_rB_j - B_rA_j) - 2h(A_r+B_j) + 4} \approx 1 \tag{30}$$

$$\theta_{c8}+\theta_{c9}+\theta_{c10} = \frac{4h^2(A_jC_r - A_rC_j)}{h^2(A_rB_j - B_rA_j) - 2h(A_r+B_j) + 4} \approx 0 \tag{31}$$

We conclude that the sum of output state coefficients of a composite load is approximately equal to 1, and the sum of input state coefficients is approximately equal to 0, which could provide a theoretical basis for validating the GDEM parameters.

IV. GDEM of Regional Power Grid

The aggregated regional power grid is illustrated in Fig. 3, in which the synchronous generator model is expressed by (11) and (12), and the composite load model is expressed by (26) and (27). The discrete-time model of the regional power grid is deduced by introducing the terminal voltage of the boundary bus and the currents injected by the external power grid as input and output state variables, respectively.

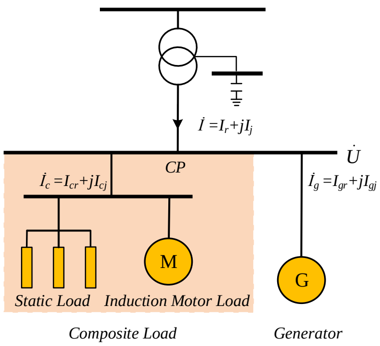

Fig. 3. Regional power grid

In Fig. 3, the current flow into the coupling point (CP) is expressed as

$$\dot{I} = \dot{I}_c + \dot{I}_g \tag{32}$$

where $\dot{I}_c$ is the current flow into the composite load, and $\dot{I}_g$ is the current flow into the synchronous generator.

The incremental form of (32) is expressed as

$$\Delta I = \Delta I_r + j\Delta I_j = \Delta I_c + \Delta I_g \tag{33}$$

We employ weighting factors to coordinate synchronous generator and composite load characteristics in the discrete-time model of a regional power grid considering by concluding that at steady state there exists a certain correlation between real and imaginary parts of the currents flowing into the synchronous generator and the composite load.

Assume that a proportion factor K_r exists between the real part of the synchronous generator current and that of the composite load, while another proportion factor K_j would apply to imaginary parts, which are stated as

$$\begin{cases} I_{cr} = K_r I_{gr} \\ I_{cj} = K_j I_{gj} \end{cases} \tag{34}$$

Considering (11), (12), (26), (27), (33), and (34), the CP current in Fig. 3 is expressed as,

$$\begin{bmatrix} \Delta I_r(k+3) \\ \Delta I_j(k+3) \end{bmatrix} = \begin{bmatrix} \theta_1 & \theta_2 & \theta_3 & 0 & 0 & 0 \\ 0 & 0 & 0 & \theta_8 & \theta_9 & \theta_{10} \end{bmatrix} \begin{bmatrix} \Delta I_r(k+2) \\ \Delta I_r(k+1) \\ \Delta I_r(k) \\ \Delta I_j(k+2) \\ \Delta I_j(k+1) \\ \Delta I_j(k) \end{bmatrix} + \begin{bmatrix} \theta_4 & \theta_5 & \theta_6 & \theta_7 \\ \theta_{11} & \theta_{12} & \theta_{13} & \theta_{14} \end{bmatrix} \begin{bmatrix} \Delta U(k+3) \\ \Delta U(k+2) \\ \Delta U(k+1) \\ \Delta U(k) \end{bmatrix} \tag{35}$$

where $\theta_1 = \dfrac{\theta_{c1} + K_r\theta_{g1}}{K_r+1}$, $\theta_2 = \dfrac{\theta_{c2} + K_r\theta_{g2}}{K_r+1}$, $\theta_3 = \theta_{g3}$, $\theta_4 = \theta_{g4} + \theta_{c3}$, $\theta_5 = \theta_{g5} + \theta_{c4}$, $\theta_6 = \theta_{g6} + \theta_{c5}$, $\theta_7 = \theta_{g7}$, $\theta_8 = \dfrac{\theta_{c6} + K_j\theta_{g8}}{K_j+1}$, $\theta_9 = \dfrac{\theta_{c7} + K_j\theta_{g9}}{K_j+1}$, $\theta_{10} = \theta_{g10}$, $\theta_{11} = \theta_{g11} + \theta_{c8}$, $\theta_{12} = \theta_{g12} + \theta_{c9}$, $\theta_{13} = \theta_{g13} + \theta_{c10}$, $\theta_{14} = \theta_{g14}$.

Based on the relationships among coefficients in (13)–(16), (28)–(31) and (33)-(34), when h is small, the following relationships among coefficients in (29) are obtained:

$$\theta_1 + \theta_2 + \theta_3 = \frac{\theta_{c1} + \theta_{c2} + K_r(\theta_{g1} + \theta_{g2} + \theta_{g3}) + \theta_{g3}}{K_r+1} \approx 1 \tag{36}$$

$$\theta_4 + \theta_5 + \theta_6 + \theta_7 = (\theta_{c3} + \theta_{c4} + \theta_{c5}) + (\theta_{g4} + \theta_{g5} + \theta_{g6} + \theta_{g7}) \approx 0 \tag{37}$$

$$\theta_8 + \theta_9 + \theta_{10} = \frac{\theta_{c6} + \theta_{c7} + K_r(\theta_{g8} + \theta_{g9} + \theta_{g10}) + \theta_{g10}}{K_r+1} \approx 1 \tag{38}$$

$$\theta_{11} + \theta_{12} + \theta_{13} + \theta_{14} = (\theta_{c8} + \theta_{c9} + \theta_{c10}) + (\theta_{g11} + \theta_{g12} + \theta_{g13} + \theta_{g14}) \approx 0 \tag{39}$$

Accordingly, we draw the following conclusions for GDEM:

1) The regional power grid model can be expressed similar to that of a synchronous generator or a composite load.

2) The coefficients of equivalent components in the regional power grid model are functions of h.

3) When h is small, the sum of output state coefficients in the regional power grid model is approximately equal to 1, and the sum of input state coefficients is approximately equal to 0, which could provide a theoretical basis for validating the estimated GDEM parameters.

We disregarded the effect of power network in our regional model derivation. Ref. [34] proposed a dynamic power system equivalent model using power transfer distribution factors. Accordingly, the model in Fig. 4 represents a regional power grid considering the regional power grid network. In Fig. 4, z_{fm} and z_{fg} are composite load and synchronous machine impedances, respectively in the network admittance matrix. When the regional power grid network is considered, the GDEM dimension will be increased.

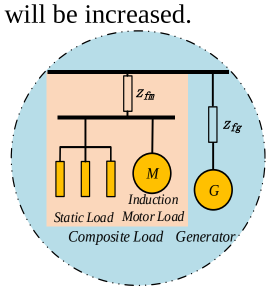

Fig. 4. Regional power grid representation considering power grid network

We can estimate the GDEM parameters using the least squares estimation method [35],[36]. Here, (35) is represented as,

$$Y = \theta\Gamma \tag{40}$$

where Γ and Y are the GDEM input and output signals, respectively, measured in the regional power grid terminal bus, and θ represents the GDEM parameters. Accordingly,

$$\boldsymbol{\Gamma} = [\Delta I_r(k+2) \quad \Delta I_r(k+1) \quad \Delta I_r(k) \quad \Delta I_j(k+2) \quad \Delta I_j(k+1) \quad \Delta I_j(k) \quad \Delta U(k+3) \quad \Delta U(k+2) \quad \Delta U(k+1) \quad \Delta U(k) \;]^T$$

$$, \; Y = \begin{bmatrix} \Delta I_r(k+3) \\ \Delta I_j(k+3) \end{bmatrix}, \; \theta = \begin{bmatrix} \theta_1 & \theta_2 & \theta_3 & 0 & 0 & 0 & \theta_4 & \theta_5 & \theta_6 & \theta_7 \\ 0 & 0 & 0 & \theta_8 & \theta_9 & \theta_{10} & \theta_{11} & \theta_{12} & \theta_{13} & \theta_{14} \end{bmatrix}.$$

To estimate the parameter θ, we apply the least squares method in which the residual J is minimized as

$$\min_{\theta} J = \left\| \hat{\theta}\boldsymbol{\Gamma} - Y \right\|^2 \tag{41}$$

where $\hat{\theta}$ are the estimated GDEM parameters.

When $\partial J / \partial \hat{\theta} = 0$, the estimated parameters $\hat{\theta}$ and output values $\hat{Y}$ are attained as,

$$\hat{\theta} = (\boldsymbol{\Gamma}^T \boldsymbol{\Gamma})^{-1} \boldsymbol{\Gamma}^T Y \tag{42}$$

$$\hat{Y} = \hat{\theta}\boldsymbol{\Gamma} \tag{43}$$

where $\hat{Y}$ is the estimated GDEM output.

According to (42) and (43), when we get the values of the $\boldsymbol{\Gamma}$ and Y from the regional power grid, the estimated parameters $\hat{\theta}$ and estimated output $\hat{Y}$ can be calculated. As GDEM is in the incremental form when estimated output $\hat{Y}$ is known, Ir and Ij in the regional power grid will be calculated by adding steady state values of Ir_0 and Ij_0, to the estimated values.

V. Simulation and Verification

In this section, two regional power grids are simulated. The results verify the accuracy and effectiveness of the proposed equivalent model for representing the regional power grids. All simulations are conducted on a computer running a 64-bit Windows 10, with a 3.6 GHz Intel (R) Core (TM) i7-7700 CPU and 8GB memory. The version 7.12 of the Power System Analysis Software Package (PSASP) software and the version R2016a of the Matlab software are used for simulation.

When GDEM is applied to a simple regional power grid with composite load for verifying the GDEM model, the steps for deriving GDEM parameters include:

1) The power system model structure with parameters for the regional power grid are presented.

2) GDEM parameters are obtained, relationships among GDEM parameters are verified, and adaptability and dynamic characteristic of GDEM are examined through derivation and estimation methods.

Case 1: Regional power grid is represented by a composite load

For a certain regional power grid, the CEPRI test system as illustrated in Fig. 5 is considered for simulation in which a composite load is connected to BUS50 in the regional power grid.

To verify the feasibility of the proposed model, typical values are utilized for representing the composite load: $R_s=0$, $R_r=0.02$, $X_s=0.18$, $X_r=0.12$, $X_m=3.5$ and $h=0.01$. A single-phase-to-ground fault is applied to the transmission line located between BUS16 and BUS19 at t=1s. The fault is cleared at t=1.2s, and the original steady state is restored. Then, the GDEM of a composite load is estimated based on (26) and (27) as:

$$\Delta I_{cr}(k+2) = 1.9976\Delta I_{cr}(k+1) - 0.9976\Delta I_{cr}(k) + 0.0088\Delta U(k+2) + 0.0000049\Delta U(k+1) - 0.0087\Delta U(k) \tag{44}$$

$$\Delta I_{cj}(k+2) = 1.9976\Delta I_{cj}(k+1) - 0.9976\Delta I_{cj}(k) - 5.8376\Delta U(k+2) + 11.6687\Delta U(k+1) - 5.83102\Delta U(k) \tag{45}$$

In order to verify the GDEM approach, the coefficients of discrete-time model of the regional power grid are also obtained by the least-square curve fitting in which the sum of squared differences between fitted values and CP current trajectories is minimized in order to estimate the coefficients.

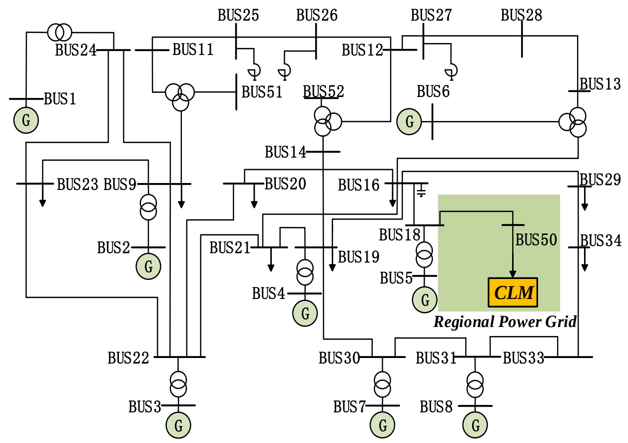

Fig. 5. Test system in Case 1

Two disturbances corresponding to the fault current are represented by voltage dips which are simulated by modifying the grounding resistance; the disturbed CP current trajectories used for estimating the coefficients in the discrete-time model are listed in Table I.

The fitted curves for real and imaginary parts of the CP current under two disturbances are depicted in Figs. 6 and 7, respectively. Here, the black curve corresponds to actual values in the terminal bus 50, the green one corresponds to estimated values using (44) and (45), and the red one corresponds to calculated values by least squares fitting based on (26) and (27). Figs. 6 and 7 show that the estimated and fitted real and the imaginary parts of currents are approximately the same as the actual curves representing subtle differences in enlarged spots.

TABLE I
Parameters in Case 1

Parameters	Values		Relationship
	3%	30%	
θ_{c1}	1.99762	1.99762	$\theta_{c1}+\theta_{c2}\approx1$
θ_{c2}	-0.99762	-0.99762	
θ_{c3}	-0.00875	-0.00875	$\theta_{c3}+\theta_{c4}+\theta_{c5}\approx0$
θ_{c4}	-0.0000007	-0.0000007	
θ_{c5}	0.00874	0.00874	
θ_{c6}	1.99762	1.99762	$\theta_{c6}+\theta_{c7}\approx1$
θ_{c7}	-0.99762	-0.99762	
θ_{c8}	-5.83766	-5.83765	$\theta_{c8}+\theta_{c9}+\theta_{c10}\approx0$
θ_{c9}	11.66874	11.66874	
θ_{c10}	-5.83106	-5.83106	

Using Table I and Figs. 6 and 7 in this case study, we conclude that:

1) The coefficients values in the Table I are close to the true coefficients values in (44)–(45), verifying the correctness of the proposed discrete-time model.

2) The coefficients are similar in the two disturbances, indicating that the proposed discrete-time model is robust against operating conditions in the external power grid.

3) The sum of output coefficients is approximately equal to 1, and the sum of input coefficients is approximately equal to 0, which accord with (28)–(31). The relationship among

coefficients provide a theoretical basis for validating GDEM parameters. In addition, the relationship among coefficients reduces the number of parameters that need to be estimated for representing GDEM. In the (28) and (30), if we know one parameter in the equation, we can determine the other one. In (29) and (31), if we know two parameters in the equation, we can get the last one.

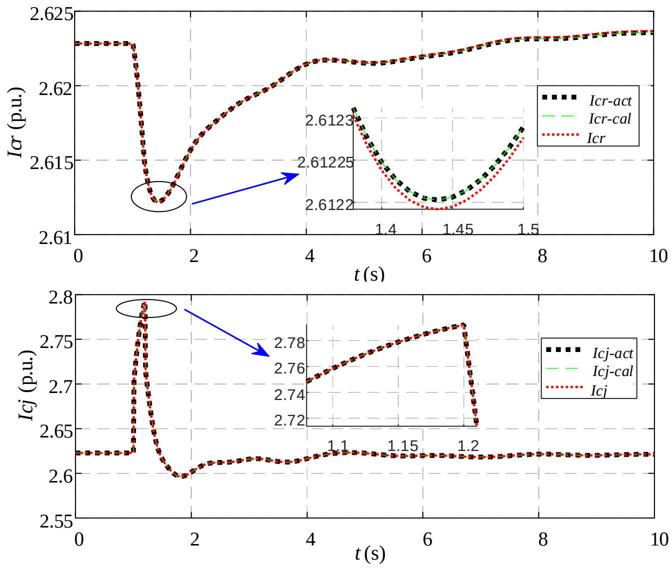

Fig. 6. Dynamic response of *Ir* and *Ij* with disturbance 1

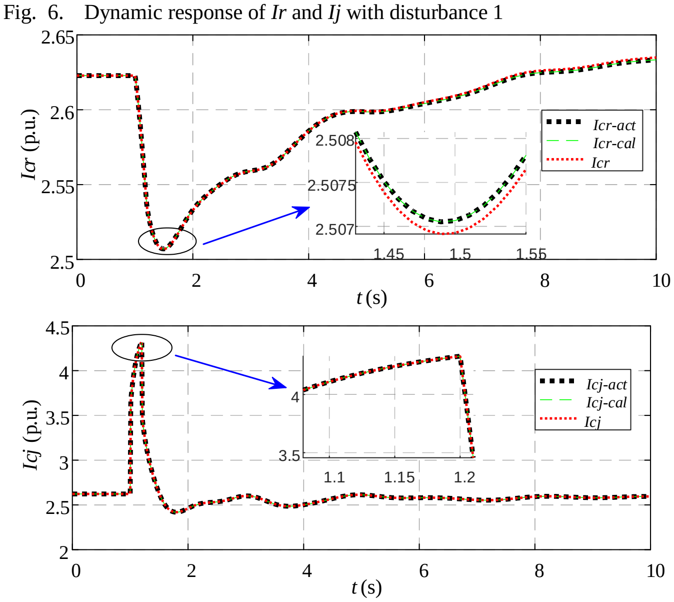

Fig. 7. Dynamic response of *Ir* and *Ij* with disturbance 2

In Case 1, the GDEM methods has been verified for through the research on GDEM consisted by composite load. When GDEM is applied to a more complex regional power grid considering the following steps,

1) The terminal voltage of boundary bus and the injected current by external grid are calculated as input and output state variables in each regional power system.

2) GDEM parameters are estimated, relationships among GDEM parameters are verified, and adaptability and dynamic characteristic of GDEM are examined through estimation methods.

Case 2: Regional power grid is represented by a synchronous generator together with a composite load

Considering another certain regional power grid, the CEPRI system, depicted in Fig. 8, is used again for simulation. The regional power grid consists of a synchronous generator and a composite load located at BUS5 and BUS50, respectively. When we consider the generator as aggregated generator and the composite load as aggregated composite load, the results will be the same. The synchronous generator is located at BUS5 and its parameters are given in Table II. The composite load is accessed at BUS50, and the proportion of the induction motor is 30%, the static load consists of constant reactance, and the induction motor parameters are given in Table III.

In this study, a single-phase-to-ground fault is applied at t=1s to the transmission line located between BUS16 and BUS19, and the fault is cleared at t=1.2s. The 3%, 20%, and 30% voltage dips are attained by setting appropriate grounding resistances.

The GDEM model parameters with these disturbances are presented in Table IV which reveal the following observations,

1) The coefficients in the discrete-time model are similar in two disturbances.

2) The sum of output state coefficients of the model is approximately equal to 1, and the sum of input state coefficients of the model is approximately equal to 0, which accord with (36)-(39). On the one hand, the relationship among coefficients provide a theoretical basis for validating GDEM parameters; on the other hand, the relationship among coefficients reduces the number of parameters that need to be estimated for representing the equivalent system. In (36) and (38), we can determine the last one parameter if we know the two parameters in the equation. In (37) and (39), we can determine the last parameter if we know the three parameters in the equation.

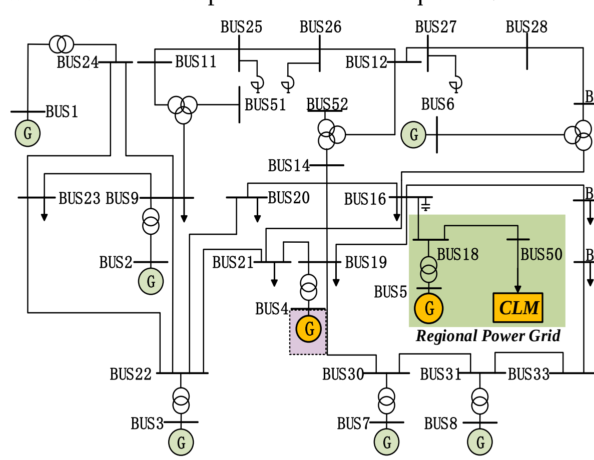

Fig. 8. Test system in Case 2

TABLE II
PARAMETERS IN SYNCHRONOUS GENERATOR LOCATED AT BUS5

X_d	X_d'	X_d''	X_q	X_q'	X_q''
1.951	0.306	0.198	1.951	1.951	0.198
T_j	T_{d0}'	T_{q0}'	T_{d0}''	T_{q0}''	D
6.149	6.2	0.1	9999	0.5	0

TABLE III
PARAMETERS IN INDUCTION MOTOR LOCATED AT BUS50

R_r	X_s	X_r	X_m	T_j	s
0.02	0.295	0.12	2	0.576	0.0116

TABLE IV
PARAMETERS IN CASE 2

Parameters	Values 3%	Values 20%	Values 30%	Relationship
θ_1	1.2437	1.9050	1.3778	$\theta_1+\theta_2+\theta_3\approx 1$
θ_2	0.1647	0.1429	0.1789	
θ_3	-0.4516	-0.3562	-0.3373	
θ_4	3.6052	3.3894	3.5042	$\theta_4+\theta_5+\theta_6+\theta_7\approx 0$
θ_5	-4.9354	-4.7539	-5.2584	
θ_6	-0.4482	-0.2083	0.4721	
θ_7	1.8312	1.3179	1.3287	
θ_8	1.2098	1.2583	1.2850	$\theta_8+\theta_9+\theta_{10}\approx 1$
θ_9	0.1538	0.1038	0.1293	
θ_{10}	-0.3986	-0.3646	-0.3461	
θ_{11}	3.6052	3.7077	3.5042	$\theta_{11}+\theta_{12}+\theta_{13}+\theta_{14}\approx 0$
θ_{12}	-4.9354	-5.0273	-5.2584	
θ_{13}	-0.4482	-0.4246	0.4721	
θ_{14}	1.8312	1.5119	1.3287	

The disturbed power system curves with GDEM model and the actual curves corresponding to two disturbances are illustrated in Figs. 9-11. In Figs. 9 and 11, the black curve is an actual value in terminal bus 50 and the red corresponds to estimated values by least squares fitting based on GDEM. In Fig. 9, the blue line is *Ir* when the regional power grid equivalent is represented by the aggregated generator. In the Fig. 9, the fitted GDEM is more accurate than the model represented by the equivalent aggregated generator.

It is possible that the proposed GDEM linearization would limit its application to a more localized section of the power system operating point. In order to demonstrate the impact of linearization, we have made a comparison of GDEM with an original nonlinear model and the corresponding results are shown here. In Fig. 10, the blue line is *Ir* when the regional power grid equivalent is represented by the original nonlinear model. In Fig. 10, the fitted GDEM is close to the model represented by the original nonlinear model and the actual value of *Ir*.

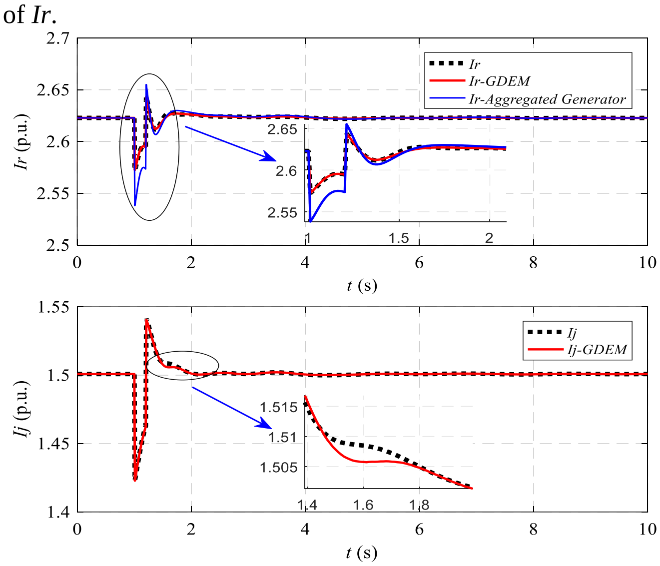

Fig. 9. Dynamic response of *Ir* and *Ij* with disturbance 1

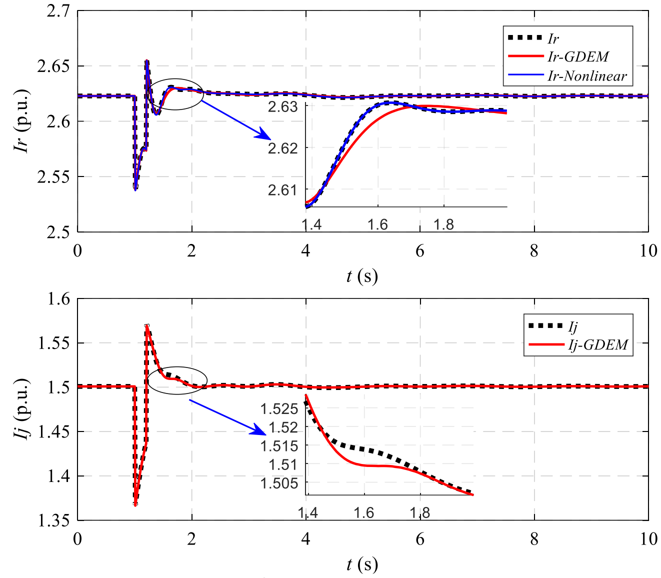

Fig. 10. Dynamic response of *Ir* and *Ij* with disturbance 2

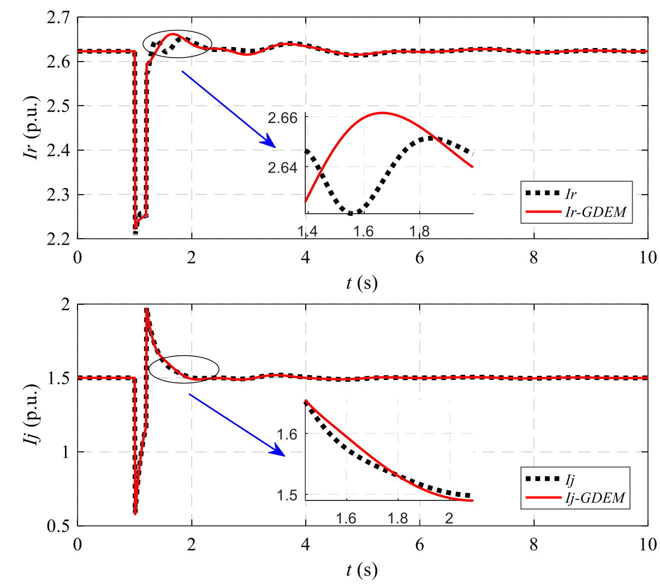

Fig. 11. Dynamic response of *Ir* and *Ij* with disturbance 3

In Case 2, GDEM is used to derive the model of the regional power grid with relatively complex components. In Fig. 11, *Ir* according to the least square fitting curves for representing GDEM cannot fit the actual *Ir* well when the regional power gird results in a 30% voltage dip in the regional power grid operating point. However, simulations and verifications in Case 2 demonstrate that GDEM can be used for the regional power grid representation when the disturbance results in a less than 30% voltage dip (which essentially covers the majority of regional power grid disturbances).

The root mean square error (RMSE) is applied to calculated the difference between actual and least square fitting curves as presented in Table V. The parameters with disturbance 1 are used in curve fitting with disturbance 2 and disturbance 3 and vice versa to verify the correctness of the model for mutual-fitting RMSE are listed in Table VI. In Figs. 9-11, the fitted curves using GDEM are approximately the same as the actual curves representing subtle differences in enlarged spots with the small RMSE listed in Table V. The mutual-fitting RMSE of *Ir* and *Ij* is small enough so that the validity and adaptability of the proposed GDEM for the regional power grid are verified.

TABLE V
RMSE FOR DISTURBED CURVES

Voltage dip	RMSE	
	Ir	*Ij*
3%	3.16e-4	3.69e-4
20%	5.06e-4	5.94e-4
30%	2.03e-3	8.87e-4

TABLE VI
MUTUAL-FITTING RMSE FOR DISTURBED CURVES

Voltage Dip	RMSE of *Ir*			RMSE of *Ij*		
	3%	20%	30%	3%	20%	30%
3%	3.16e-4	5.62e-4	2.25e-3	3.69e-4	1.33e-3	6.02e-4
20%	7.84e-4	5.06e-4	1.01e-3	4.48e-4	8.86e-4	6.47e-4
30%	4.05e-4	1.63e-3	2.03e-3	1.12e-3	3.84e-4	8.87e-4

In this case, we made a simulation to consider voltage phase angle variation. The generator located at BUS4 is chosen as a study object with parameters given in Table VII. The same single-phase-to-ground fault is applied at t=1s to the transmission line located between BUS16 and BUS19 and the fault is cleared at t=1.2s with a 20% voltage dip. The least square fitting results are shown in Fig. 12 for the real part of the generator current at terminal Bus 4, where the black curve *Igr-actual* is the actual values of *Igr*, the blue curve *Igr'* and the red curve *Igr* are with and without voltage phase angle variations which are estimated values by least squares fitting based on (11) and (19), respectively.

TABLE VII
PARAMETERS OF SYNCHRONOUS GENERATOR LOCATED AT BUS4

X_d	X_d'	X_d''	X_q	X_q'	X_q''
1.81	0.284	0.183	1.81	1.81	0.183
T_j	T_{d0}'	T_{q0}'	T_{d0}''	T_{q0}''	D
66.672	6.2	0.192	9999	1.89	0

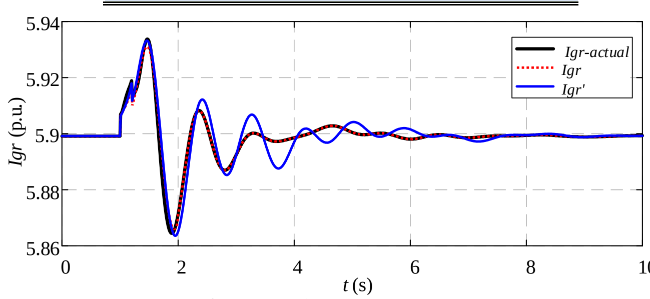

Fig. 12. Comparison of *Igr-actual, Igr, Igr'*

In Fig. 12, the RMSE of *Igr-actual* with *Igr* and *Igr'* are 1.15e-3 and 3.15e-3, respectively. Accordingly, the fitting accuracy in the simulation is not improved when the bus voltage phase angle is considered. Furthermore, the number of parameters would be increased when the variations in bus voltage phase angle are explicitly expressed in (7). Correspondingly, the variations are ignored in our study in order to facilitate the derivation and the simulation of the proposed model.

Case 3: A regional power grid of Central China

In Cases 1 and 2, we make a GDEM verification in which we apply GDEM to a regional power grid of central China (see Fig. 13). On 03-08-2016, a single-phase-to-ground fault occurred in the 500Kv line between buses 12 and 19. The fault measurement (terminal voltage, terminal active and reactive power) of the regional power grid are provided by phase measurement units (PMUs).

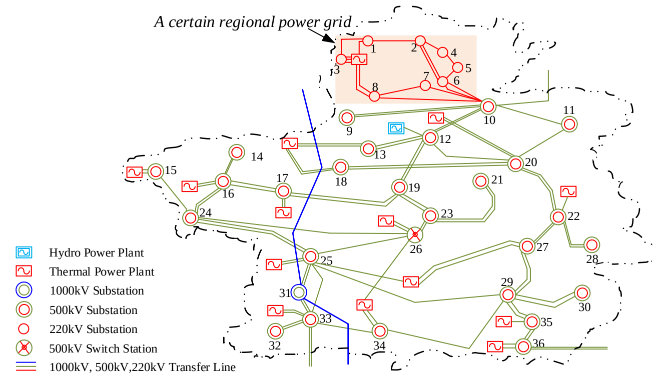

Fig. 13. Topology of the regional power grid of central China

Here are steps to verify the GDEM in the case study, in which we have made a comparison of actual fault measurements and those obtained through the GDEM application.

1) Collect the steady state PMU measurements of the regional power grid.
2) Use the steady state measurement values to estimate the GDEM parameters (see Table VIII) by least square fitting method.
3) Use the voltage dip fault values in the regional power grid measured by PMUs and apply the GDEM obtained in Step 2 to calculate the dynamic response of *Ir* and *Ij*.
4) Compare the PMU fault measurements with the GDEM values.

In Table VIII, we also find that the sum of output coefficients is approximately equal to 1, and the sum of input coefficients is approximately equal to 0 in the regional power grid of Central China, which provide a theoretical basis for validating the corresponding GDEM parameters. The RMSE of *Ir* and *Ij* in Case 3 are 4.69e-3 and 9.48e-3, respectively, which demonstrate that the dynamic response of *Ir* and *Ij* obtained through GDEM in Step 2 are almost the same as those of actual PMU measurements in a certain stable range. The Case of the regional power grid of central China has exhibited and verified the application of GDEM.

TABLE VIII
PARAMETERS IN CASE 3

Parameter	Value	Relationship
θ_1	0.9423	$\theta_1+\theta_2+\theta_3\approx 1$
θ_2	-0.062	
θ_3	0.0354	
θ_4	-0.1984	$\theta_4+\theta_5+\theta_6+\theta_7\approx 0$
θ_5	0.347	
θ_6	-0.2522	
θ_7	0.1134	
θ_8	1.0957	$\theta_8+\theta_9+\theta_{10}\approx 1$
θ_9	-0.1624	
θ_{10}	-0.0297	
θ_{11}	-2.4385	$\theta_{11}+\theta_{12}+\theta_{13}+\theta_{14}\approx 0$
θ_{12}	2.2912	
θ_{13}	-0.4643	
θ_{14}	0.2745	

In Step 3, voltage dip occurs in the regional power grid of central China as depicted in Fig. 14. The corresponding dynamic response of *Ir* and *Ij* are depicted in Figs. 15 and 16.

Figs. 14-16 show that actual PMU measurements included some ripples around the steady state value which are from power electronic devices and electromagnetic transient properties. The proposed power grid has a self-healing capability which allows voltages and active and reactive power in the regional power grid of central China to recover its steady state quickly when the single-phase-to-ground fault occurs.

Other potential applications of GDEM indicate that GDEM is not only conducive to the assembly of regional power system models for real-time analyses that guide the secure operation of large scale power systems but could also be used for the equivalent modeling of a host of distributed AC/DC microgrids and the generalized load modeling and simulation in large-scale power systems. Some of these topics will be analyzed further in our future studies.

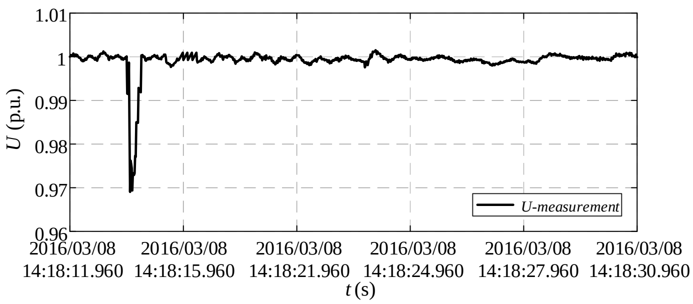

Fig. 14. Voltage dip in the regional power grid of central China

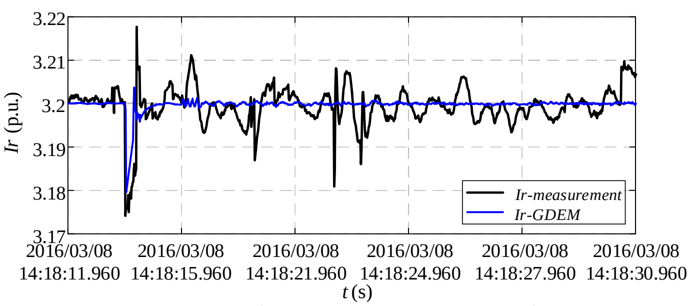

Fig. 15. Dynamic response of *Ir* in the regional power grid of central China

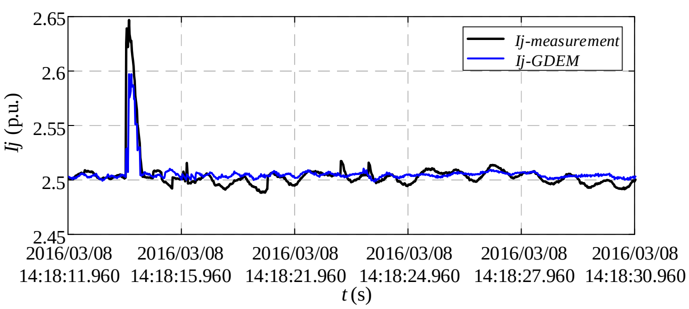

Fig. 16. Dynamic response of *Ij* in regional power grid of central China

VI. Conclusion

In this paper, a GDEM is developed for regional power grids which encompasses the fundamental models of synchronous generators and composite loads. The inherent relationships among GDEM coefficients in a discrete-time models are introduced which are linked with coefficients associated with electric power components. As shown in case studies, using the GDEM coefficients produce current trajectories that are very similar to the actual power system cases. Simulation results also validate the relationships among coefficients in the proposed GDEM for the regional power grids. The case study pertaining to the regional power grid of central China verified the application of GDEM.

References

[1] P. Ju, L. Q. Ni, and F. Wu, "Dynamic equivalents of power systems with online measurements. Part 1," *IEE Proceedings-Generation, Transm. Distrib.*, vol. 152, no. 1, pp. 109–114, 2005.

[2] M. Shahidehpour, Z. Li, S. Bahraamirad, Z. Li, and W. Tian, "Networked microgrids: Exploring the possibilities of the IIT-bronzeville grid," *IEEE Power Energy Mag.*, vol. 15, no. 4, pp. 63–71, 2017.

[3] X. Liu, M. Shahidehpour, Z. Li, X. Liu, Y. Cao, and Z. Bie, "Microgrids for enhancing the power grid resilience in extreme conditions," *IEEE Trans. Smart Grid*, vol. 8, no. 2, pp. 589–597, 2017.

[4] F. Milano, "Small-signal stability analysis of large power systems with inclusion of multiple delays," *IEEE Trans. Power Syst.*, vol. 31, no. 4, pp. 3257–3266, 2016.

[5] A. Ortega and F. Milano, "Modeling, simulation and comparison of control techniques for energy storage systems," *IEEE Trans. Power Syst.*, vol. 32, no. 3, pp. 2445–2454, 2016.

[6] N. Kishor, J. M. Seppänen, J. Turunen, A.-J. Nikkilä, L. C. Haarla, and S. Purwar, "Low-order controller design using remotely measured time delayed signals for stabilisation of equivalent power grid," *IET Gener. Transm. Distrib.*, vol. 9, no. 16, pp. 2575–2585, 2015.

[7] Z. Liu, D. Li, and S. Liu, "Study on dynamic equivalence and modeling of regional power grid based on RTDS," in *IEEE Powertech*, 2013, pp. 1–6.

[8] A. Vahidnia, G. Ledwich, E. Palmer, and A. Ghosh, "Generator coherency and area detection in large power systems," *IET Gener. Transm. Distrib.*, vol. 6, no. 9, p. 874, 2012.

[9] S. Kim, S. Member, and T. J. Overbye, "Enhanced measurement-based dynamic equivalence using coherency identification," in *IEEE Power and Energy Conf. at Illinois*, 2013, pp. 200–205.

[10] M. A. Mcthod, "Modified selective modal analysis method and its application in the analysis of power system dynamics," *IEEE Trans. Power Syst.*, vol. 6, no. 3, pp. 1189–1195, 1991.

[11] R. M. Lin, "Development of a new and effective modal identification method-mathematical formulations and numerical simulations," *J. Vib. Control*, vol. 17, no. 5, pp. 741–758, 2011.

[12] B. Zhang, Y. Zhang, M. Liao, and Y. Xie, "Study on dynamic equivalent coherency-based of Hainan power grid," in *Power and Energy Engineering Conference*, 2012, no. 1, pp. 2–5.

[13] M. Shiroei, B. Mohammadi-Ivatloo, and M. Parniani, "Low-order dynamic equivalent estimation of power systems using data of phasor measurement units," *Int. J. Electr. Power Energy Syst.*, vol. 74, no. 7, pp. 134–141, 2016.

[14] S. Yu, S. Zhang, and X. Zhang, "Two-step method for the online parameter identification of a new simplified composite load model," *IET Gener. Transm. Distrib.*, vol. 10, no. 16, pp. 4048–4056, 2016.

[15] IEEE Task Force, "Load representation for dynamic performance analysis," *IEEE Trans. Ind. Appl.*, vol. 8, no. 2, pp. 472–482, 1993.

[16] P. Ju *et al.*, "Composite load models based on field measurements and their applications in dynamic analysis," *Gener. Transm. Distrib. IET*, vol. 1, no. 5, pp. 724–730, 2007.

[17] D. N. Kosterev, C. W. Taylor, and W. a. Mittelstadt, "Model validation for the August 10, 1996 WSCC system outage," *IEEE Trans. Power Syst.*, vol. 14, no. 3, pp. 967–979, 1999.

[18] C. Qin, P. Ju, F. Wu, Y. Liu, X. Ye, and G. Wu, "An efficient multi-area networks-merging model for power system online dynamic modeling," *CSEE J. Power Energy Syst.*, vol. 1, no. 4, pp. 37–43, 2015.

[19] P. Ju, E. Handschin, and D. Karlsson, "Nonlinear dynamic load modelling: model and parameter estimation," *IEEE Trans. Power Syst.*, vol. 11, no. 4, pp. 1689–1697, 1996.

[20] J. V. Milanovic and S. Mat Zali, "Validation of equivalent dynamic model of active distribution network cell," *IEEE Trans. Power Syst.*, vol. 28, no. 3, pp. 2101–2110, 2013.

[21] S. M. Zali and J. V. Milanović, "Dynamic equivalent model of distribution network cell using prony analysis and nonlinear least square optimization," in *2009 IEEE Bucharest PowerTech: Innovative Ideas Toward the Electrical Grid of the Future*, 2009, pp. 1–6.

[22] H. Chen, C. Deng, and D. Li, "Recurrent neural network-based dynamic equivalencing in power system," *2007 IEEE Int. Conf. Control Autom.*, vol. 0, pp. 2396–2399, 2007.

[23] A. Chang and M. M. ADIBI, "Power system dynamic equivalents," *IEEE Trans. Power Appar. Syst.*, vol. PAS-89, no. 8, pp. 1737–1744, 1970.

[24] F. Milano, "Semi-implicit formulation of differential-algebraic equations for transient stability analysis," *IEEE Trans. Power Syst.*, vol. 31, no. 6, pp. 4534–4543, 2016.

[25] F. Milano, "An open source power system analysis toolbox," *IEEE Trans. Power Syst.*, vol. 20, no. 3, pp. 1–8, 2005.

[26] A. Chakrabortty, J. H. Chow, and A. Salazar, "A measurement-based framework for dynamic equivalencing of large power systems using wide-area phasor measurements," *IEEE Trans. Smart Grid*, vol. 2, no. 1, pp. 56–69, 2011.

[27] H. Wu, J. Hu, and Y. Xie, "Characteristic model-based all-coefficient adaptive control method and its applications," *IEEE Trans. Syst. Man Cybern. Part C Appl. Rev.*, vol. 37, no. 2, pp. 213–221, 2007.

[28] T. Sugiyama, T. Nishiwaki, S. Takeda, and S. Abe, "Measurements of synchronous machine parameters under operating condition," *IEEE Trans. Power Appar. Syst.*, no. 4, pp. 895–904, 1982.

[29] P. Kundur, "Power system stability and control," New York: McGraw-hill, 1994, pp. 139–168.

[30] F. Shen, P. Ju, L. Gu, X. Huang, B. Lou, and H. Huang, "Mechanism analysis of power load using difference equation approach," in *2016 IEEE International Conference on Power System Technology*, 2016, pp. 1–6.

[31] J. Ma, D. Han, R. M. He, Z. Y. Dong, and D. J. Hill, "Reducing identified parameters of measurement-based composite load model," *IEEE Trans. Power Syst.*, vol. 23, no. 1, pp. 76–83, 2008.

[32] C. Cai, Y. Jin, Y. Yu, and P. Ju, "Load modeling with considering frequency characteristic," *Sustain. Power Gener. Supply*, pp. 1–6, 2012.

[33] P. Ju, "The theory and method of power system modeling," Nanjing: China Science Press, 2010, pp. 154–260.

[34] F. Milano and K. Srivastava, "Dynamic REI equivalents for short circuit and transient stability analyses," *Electr. Power Syst. Res.*, vol. 79, no. 6, pp. 878–887, 2009.

[35] Y. Wehbe, L. Fan, and Z. Miao, "Least squares based estimation of synchronous generator states and parameters with phasor measurement units," in *2012 North American Power Symposium*, 2012, pp. 1–6.

[36] S. Nabavi and A. Chakrabortty, "Structured identification of reduced-Order models of power systems in a differential-algebraic form," *IEEE Trans. Power Syst.*, vol. 32, no. 1, pp. 198–207, 2017.

APPENDICES

A. Specific parameters of (7) and (8)

$$a_{gr} = \frac{1}{2}\sin 2\delta_0 (X_q T_q'' T_{d0}'' T_{d0}' - X_d T_d'' T_d' T_{q0}''),$$

$$b_{gr} = \frac{1}{2}\sin 2\delta_0 \begin{bmatrix} X_q T_q''(T_{D0}' + T_{d0}') + T_{d0}'' T_{d0}' X_q - \\ X_d T_d'' T_d' - X_d (T_D' + T_d') T_{q0}'' \end{bmatrix},$$

$$c_{gr} = \frac{1}{2}\sin 2\delta_0 \left[(T_{D0}' + T_{d0}') X_q - X_d (T_D' + T_d') - T_{q0}'' X_d \right],$$

$$d_{gr} = \frac{1}{2}\sin 2\delta_0 (X_q T_q'' + X_q - X_d),$$

$$e_{gr} = X_q T_q'' X_d T_d'' T_d', \quad f_{gr} = X_q T_q'' X_d (T_D' + T_d') + X_d T_d'' T_d' X_q,$$

$$g_{gr} = X_q T_q'' X_d + X_d X_q (T_D' + T_d'), \quad h_{gr} = X_d X_q,$$

$$a_{gj} = -\frac{1}{2}\cos 2\delta_0 \left[X_q T_q'' T_{d0}'' T_{d0}' - X_d T_d'' T_d' T_{q0}'' \right] + \frac{1}{2}\left[X_q T_q'' T_{d0}'' T_{d0}' - 3X_d T_d'' T_d' T_{q0}'' \right],$$

$$b_{gj} = -\frac{1}{2}\cos 2\delta_0 \begin{bmatrix} X_q T_q''(T_{D0}' + T_{d0}') + T_{d0}'' T_{d0}' X_q - \\ X_d T_d'' T_d' - X_d (T_D' + T_d') T_{q0}'' \end{bmatrix} + \frac{1}{2}\begin{bmatrix} X_q T_q''(T_{D0}' + T_{d0}') + T_{d0}'' T_{d0}' X_q - \\ 3X_d T_d'' T_d' - 3X_d (T_D' + T_d') T_{q0}'' \end{bmatrix},$$

$$c_{gj} = -\frac{1}{2}\cos 2\delta_0 \left[(T_{D0}' + T_{d0}') X_q - X_d (T_D' + T_d') - T_{q0}'' X_d \right] + \frac{1}{2}\left[(T_{D0}' + T_{d0}') X_q - 3X_d (T_D' + T_d') - 3T_{q0}'' X_d \right],$$

$$d_{gj} = -\frac{1}{2}\cos 2\delta_0 (X_q T_q'' + X_q - X_d) + (X_q T_q'' + X_q - 2X_d),$$

$$e_{gj} = X_q T_q'' X_d T_d'' T_d', \quad f_{gj} = X_q T_q'' X_d (T_D' + T_d') + X_d T_d'' T_d' X_q,$$

$$g_{gj} = X_q T_q'' X_d + X_d X_q (T_D' + T_d'), \quad h_{gj} = X_d X_q.$$

B. Specific parameters of (9) and (10)

$$\theta_{g1} = \frac{-3h_{gr}h^3 - 2g_{gr}h^2 + 4f_{gr}h + 24e_{gr}}{h_{gr}h^3 + 2g_{gr}h^2 + 4f_{gr}h + 8e_{gr}},$$

$$\theta_{g2} = \frac{-3h_{gr}h^3 + 2g_{gr}h^2 + 4f_{gr}h - 24e_{gr}}{h_{gr}h^3 + 2g_{gr}h^2 + 4f_{gr}h + 8e_{gr}},$$

$$\theta_{g3} = \frac{-h_{gr}h^3 + 2g_{gr}h^2 - 4f_{gr}h + 8e_{gr}}{h_{gr}h^3 + 2g_{gr}h^2 + 4f_{gr}h + 8e_{gr}},$$

$$\theta_{g4} = \frac{d_{gr}h^3 + 2c_{gr}h^2 + 4b_{gr}h + 8a_{gr}}{h_{gr}h^3 + 2g_{gr}h^2 + 4f_{gr}h + 8e_{gr}},$$

$$\theta_{g5} = \frac{3d_{gr}h^3 + 2c_{gr}h^2 - 4b_{gr}h - 24a_{gr}}{h_{gr}h^3 + 2g_{gr}h^2 + 4f_{gr}h + 8e_{gr}},$$

$$\theta_{g6} = \frac{3d_{gr}h^3 - 2c_{gr}h^2 - 4b_{gr}h + 24a_{gr}}{h_{gr}h^3 + 2g_{gr}h^2 + 4f_{gr}h + 8e_{gr}},$$

$$\theta_{g7} = \frac{d_{gr}h^3 - 2c_{gr}h^2 + 4b_{gr}h - 8a_{gr}}{h_{gr}h^3 + 2g_{gr}h^2 + 4f_{gr}h + 8e_{gr}},$$

$$\theta_{g8} = \frac{-3h_{gj}h^3 - 2g_{gj}h^2 + 4f_{gj}h + 24e_{gj}}{h_{gj}h^3 + 2g_{gj}h^2 + 4f_{gj}h + 8e_{gj}},$$

$$\theta_{g9} = \frac{-3h_{gj}h^3 + 2g_{gj}h^2 + 4f_{gj}h - 24e_{gj}}{h_{gj}h^3 + 2g_{gj}h^2 + 4f_{gj}h + 8e_{gj}},$$

$$\theta_{g10} = \frac{-h_{gj}h^3 + 2g_{gj}h^2 - 4f_{gj}h + 8e_{gj}}{h_{gj}h^3 + 2g_{gj}h^2 + 4f_{gj}h + 8e_{gj}},$$

$$\theta_{g11} = \frac{d_{gj}h^3 + 2c_{gj}h^2 + 4b_{gj}h + 8a_{gj}}{h_{gr}h^3 + 2g_{gr}h^2 + 4f_{gr}h + 8e_{gr}},$$

$$\theta_{g12} = \frac{3d_j h^3 + 2c_j h^2 - 4b_j h - 24a_j}{h_{gj}h^3 + 2g_{gj}h^2 + 4f_{gj}h + 8e_{gj}},$$

$$\theta_{g13} = \frac{3d_{gj}h^3 - 2c_{gj}h^2 - 4b_{gj}h + 24a_{gj}}{h_{gj}h^3 + 2g_{gj}h^2 + 4f_{gj}h + 8e_{gj}},$$

$$\theta_{g14} = \frac{d_{gj}h^3 - 2c_{gj}h^2 + 4b_{gj}h - 8a_{gj}}{h_{gj}h^3 + 2g_{gj}h^2 + 4f_{gj}h + 8e_{gj}}.$$

C. Specific parameters of (20) and (21)

$$\theta_{c1} = \frac{2h^2(B_rA_j - A_rB_j)+8}{h^2(A_rB_j - B_rA_j) - 2h(A_r + B_j) + 4},$$

$$\theta_{c2} = \frac{h^2(B_rA_j - A_rB_j) - 2h(A_r + B_j) - 4}{h^2(A_rB_j - B_rA_j) - 2h(A_r + B_j) + 4},$$

$$\theta_{c3} = \frac{h^2(B_rC_j - B_jC_r) - 2h(GB_j + B_rB - C_r) + 4G}{h^2(A_rB_j - B_rA_j) - 2h(A_r + B_j) + 4},$$

$$\theta_{c4} = \frac{2h^2(B_rC_j - B_jC_r) - 8G}{h^2(A_rB_j - B_rA_j) - 2h(A_r + B_j) + 4},$$

$$\theta_{c5} = \frac{h^2(B_rC_j - B_jC_r) + 2h(GB_j + B_rB - C_r) + 4G}{h^2(A_rB_j - B_rA_j) - 2h(A_r + B_j) + 4},$$

$$\theta_{c6} = \frac{2h^2(A_jB_r - B_jA_r)+8}{h^2(A_rB_j - B_rA_j) - 2h(A_r + B_j) + 4},$$

$$\theta_{c7} = \frac{h^2(A_jB_r - B_jA_r) - 2h(B_j + A_r) - 4}{h^2(A_rB_j - B_rA_j) - 2h(A_r + B_j) + 4},$$

$$\theta_{c8} = \frac{h^2(A_jC_r - A_rC_j) - 2h(-BA_r - GA_j - C_j) - 4B}{h^2(A_rB_j - B_rA_j) - 2h(A_r + B_j) + 4},$$

$$\theta_{c9} = \frac{2h^2(A_jC_r - A_rC_j) + 8B}{h^2(A_rB_j - B_rA_j) - 2h(A_r + B_j) + 4},$$

$$\theta_{c10} = \frac{h^2(A_jC_r - A_rC_j) + 2h(-BA_r - GA_j - C_j) - 4B}{h^2(A_rB_j - B_rA_j) - 2h(A_r + B_j) + 4}.$$

BIOGRAPHIES

Fu Shen (S'16) received the B.S. degrees in Hohai University and he is currently an MD-PhD student of Electrical Engineering at Hohai University, Nanjing, 211100, China. He works as research scholar in the Illinois Institute of Technology (IIT), Chicago. His research interests include modeling and control of power system.

Ping Ju (M'95–SM'10) received the B.Sc. and M.Sc. degrees from Southeast University, Nanjing, China in 1982 and 1985, respectively, and the Ph.D. degree from Zhejiang University, Hangzhou, China. From 1994 to 1995, he was an Alexander von Humboldt Fellow at the University of Dortmund, Germany. He is currently a Professor of Electrical Engineering at Hohai University, Nanjing, China. His research interests include the modeling and control of power systems. He has published five research books and authored and coauthored over 200 journal papers. Prof. Ju received the Scientific Funds for Outstanding Young Scientists of China.

Mohammad Shahidehpour (F'01) received the Honorary Doctorate degree from the Polytechnic University of Bucharest, Bucharest, Romania. He is a University Distinguished Professor and Bodine Chair Professor and Director of the Robert W. Galvin Center for Electricity Innovation at Illinois Institute of Technology. He is a member of the US National Academy of Engineering and a Fellow of the American Association for the Advancement of Science (AAAS).

Zhiyi Li (GSM'14-M'17) received the B.S. degree in electrical engineering from Xi'an Jiaotong University, Xi'an, China, in 2011 and the M.S. degree in electrical engineering from Zhejiang University, China, in 2014. He completed his Ph.D. degree in 2017 in the Electrical and Computer Engineering Department at Illinois Institute of Technology. He is a visiting faculty in the Robert W. Galvin Center for Electricity Innovation at Illinois Institute of Technology.

XuePing Pan received the Ph.D. degree from Zhejiang University, Hangzhou, China, in 2008. She is presently a professor in the College of Energy and Electrical Engineering, Hohai University, Nanjing, China. Her research interests include modeling of renewable power generation system, power system dynamic analysis, etc.